Effect of Polyamide-12 Material Compositions on Mechanical Properties and Surface Morphology of SLS 3D Printed Part

Mohammad Rafi Omar[1], Muhammad Ilman Hakimi Chua Abdullah[2], Mohd Rizal Alkahar[3], Rohana Abdullah[4], Mohd Fadzli Abdollah[5], Mahananthan Subramaniam[6], Rizwana Seeni Ibramsa[7]*

[1,2,4,6]Fakulti Teknologi Kejuruteraan Mekanikal dan Pembuatan, Universiti Teknikal Malaysia Melaka, Hang Tuah Jaya, 76100 Durian Tunggal, Melaka, Malaysia.

[1,2,3,4,5,7]Centre for Advanced Research on Energy, Universiti Teknikal Malaysia Melaka, Hang Tuah Jaya, 76100 Durian Tunggal, Melaka, Malaysia.

[1,3,5,7]Fakulti Kejuruteraan Mekanikal, Universiti Teknikal Malaysia Melaka, Hang Tuah Jaya, 76100 Durian Tunggal, Melaka, Malaysia.
** ilmanhakimi@utem.edu.my*

ABSTRACT

Despite the fact that many 3D printed products have been developed, there are still issues with the printed product's physical properties and surface morphology. This study examines the effects of significant Selective Laser Sintering (SLS) 3D printer parameters on the material strength of Polyamide-12 (PA-12). A variety of virgin materials, reheat materials, and recycled materials were used for the PA-12 material compositions. The test specimens were prepared at different process parameters and material composition percentages using the SLS 3D printer. The tensile strength, surface roughness, and surface morphology were tested. These samples were tested in accordance with ASTM D638-(IV) for tensile strength and roughness using a 10 mm x 10 mm coated sample prepared for scanning in an electron microscope. The tensile test results showed that the composition of the 100% virgin (CP1)

ISSN 1823-5514, eISSN 2550-164X

Received for review: 2021-05-10
Accepted for publication: 2021-08-27
Published: 2022-01-15

material samples appeared to be stiffer, with a lower plastic deformation at maximum tensile stress (45 MPa) and a smoother surface roughness (10.75µm). Furthermore, the SEM results showed that the specimens were partially melted with a significant amount of PA-12 powder before being sintered and coalesced.

Keywords: *3D Printing; Additive Manufacturing; Selective Laser Sintering*

Introduction

Additive manufacturing (AM) techniques offer the efficiency of the bottom-up development of 3D structures by selectively inserting material based on CAD data. These techniques have become faster, cheaper, more cost-effective, complex, better in resolution and quality [1]-[3]. AM has the potential to improve the efficiency of various industrial sectors while also serving as a valuable resource for aerospace, automotive, and biomedical engineering [3]-[5]. The variety of materials that can be used today include metals, ceramics, polymers (thermoplastics, thermosets, hydrogels), and some composite materials, such as magnetic particles, in polymer sand cells suspended in hydrogels [1, 6]. However, it is necessary to select the right AM technology by taking into account factors such as the type of product, material properties, volume, production time and cost [7, 8].

This research focuses on a specific type of 3D printing machine, the Farsoon FS402P Selective Laser Sintering (SLS) technology model. The advantages of using this SLS machine include durable parts for functional testing or low-volume production, as well as a low cost with applications in a wide range of industries including aerospace, automotive, medical consumer products, and electronics [9].

Since SLS involves the creation of parts with no supports, the design possibilities are nearly infinite. In contrast to standard melting with high shear mixing and fluidity, SLS technology does not compact during processing, making it an essential 3D printing technique for the fabrication of porous segregated structures [10]. SLS uses a CO_2 laser as the heat source to fuse the powders under pressure-free conditions [11]. The main materials used in SLS are polyamide (PA-12), poly (ethylene terephthalate) PET, and poly (ether ether ketone) PEEK. Material properties like particle size distribution, crystallinity, powder flowability, melting temperature, and melt viscosity, as well as process parameters such as faster rate and path, laser power, and ambient bed temperature all play an important role in determining the part quality and results [12]. The sintering process and product properties (surface roughness, dimensional accuracy, tensile properties, flexural properties, and time of manufacturing) are all affected by the laser processing parameters.

Both the external layers (contour of the object) and the product interior layers (hatching) can have their processing parameters changed separately. Furthermore, the amount of energy density fuel fed to the reactor determines the mechanical properties of the product. Based on the existing literature and experiments performed by other researchers, the processing conditions can be calculated using energy density [7]. However, the findings showed that high laser speeds reduced the amount of time the powder exposure to the beam, which led to poor mechanical strength of the printed structure. Thus, SLS printability is influenced by the laser energy density (ED) by altering the temperature of the powder bed [13]. Therefore, the SLS 3D parameter can have an effect on the quality of the produced part. The energy density parameter can be calculated using this formula [13, 14]:

$$ED = \frac{P}{\upsilon * h * d} \tag{1}$$

ED	energy density, J/mm^2
P	laser power, W
υ	laser beam speed, mm/s
h	scan spacing, hatch distance, mm
d	laser beam diameter, mm

Thermoplastic polymer materials are the most commonly used in the SLS machines because of their ability to be recycled [15]. PA-12 has become the most commonly used thermoplastic material due to its supercooling window, small crystallisation shrinkage, and stable processing [16]. There are four main types of nylon or PA-12 materials; glass bead nylon, carbon fiber nylon and mineral-filled nylon [17]. Farsoon Technologies have developed a thermoplastic semi-crystalline polymer material based on PA-12 and SLS FS 3300PA parts, which has good mechanical properties and is manufactured to high quality standards [18]. However, the composition (CP) of the powder will affect the shape, strength, and capability of the powder discharge [13]. PA-12, commonly used in the SLS processes, melts and crystallises (during cooling) at a wide range of temperatures. The temperature ranges are referred to in terms of SLS windows and having a wide sintering window reduces the impact of crystallisation during the printing process. A stable crystallisation during the printing process prevents shrinkage and warpage of the printed part [16]. Normally during the SLS printing process using a maximum laser beam power of 100W and oxygen level of 20%, approximately 5 to 20 percent of the powders are used to produce the parts, while the rest are required to support the parts. Therefore, the recycling of un-sintered powders is beneficial to reduce costs. Unfortunately, the molecular properties and the particle

durability limit recycling. Hence, PA-12 is relatively easy to recycle and is frequently used in the SLS production. In addition, some studies have shown that un-sintered polyamide powders (recycle powder) are affected by exposure to elevated temperatures during SLS [2]. However, the exact relationship is hard to quantify [19].

This study aims to investigate the effects of different PA-12 compositions on the mechanical properties and surface morphology using the SLS printed samples. These printed parts' properties are essential in both manufacturing and prototyping applications and are mainly influenced by the process parameters.

Methodology

Figure 1 shows the experimental approach to examine the mechanical properties of PA-12 material. All preparation and testing of samples adhered to the American Society for Testing and Materials (ASTM) standard.

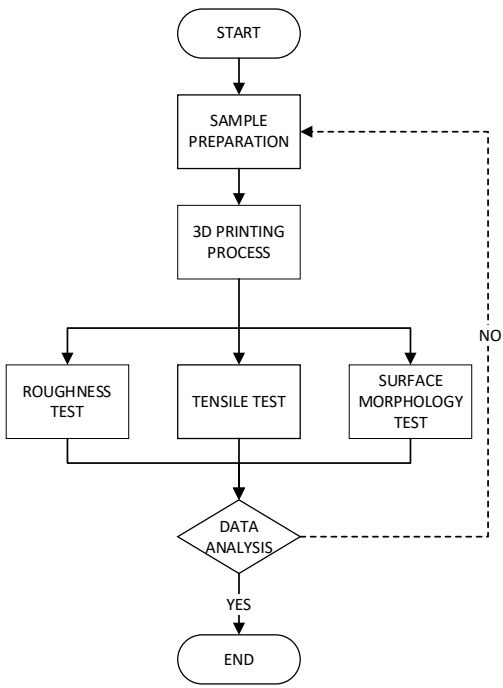

Figure 1: Experimental approach.

Specimen preparation

The specimens were prepared using three different composition percentages (CP) of PA-12 material, as shown in Table 1. Table 2 shows the mechanical characteristics of virgin PA-12 material as verified by the manufacturer. The PA-12 material was then compared between virgin and recycled powders. The results showed that scratched samples sintered with virgin powder were more fractured with smaller and smoother spheres than the adhered powder samples [2].

Table 1: PA-12 Composition percentage

Composition (CP)	(%) Virgin	(%) Reheat	(%) Recycled
1	100	0	0
2	40	20	40
3	0	0	100

*Virgin: material refers to a new manufacturer's material

*Reheat: material heating in the powder feeder chamber but never exposed to the laser beam (overflow powder)

*Recycled: un-sintering material and exposed to laser beam

Table 2: PA-12 mechanical properties based on manufacturer's data

Properties	Value
Density	0.95 g/cm^3
Tensile strength	48.1 MPa
Impact strength	3.6 KJ/m^2

Figure 2 presents the tensile test carried out on the five CP specimens printed with the SLS 3D printer in accordance with the ASTM D638 type III [20]. As shown in Figure 3, the five specimens were printed along the XY plane orientation. According to Yao [21], orientation is also an influencing factor to increase the printed part tensile strength.

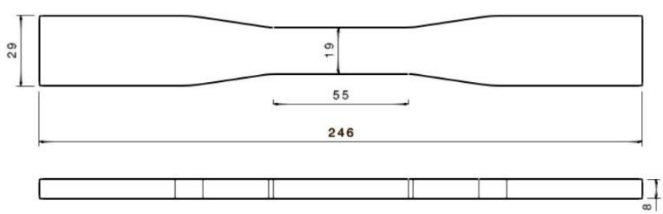

Figure 2: Tensile test ASTM D638 type III specimen.

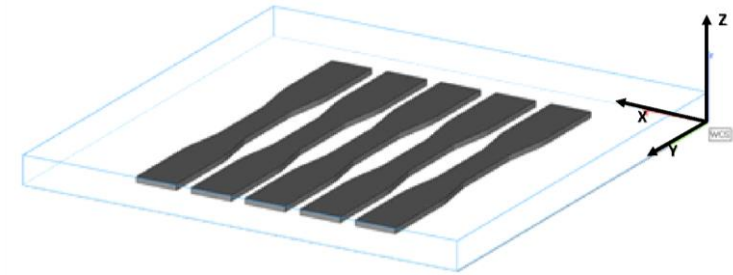

Figure 3: The printed specimens in a XY plane orientation.

Three CP specimens printed using the SLS 3D printer were prepared for the roughness test. The top layer surface roughness test locations of the printed specimen are shown in Figure 4.

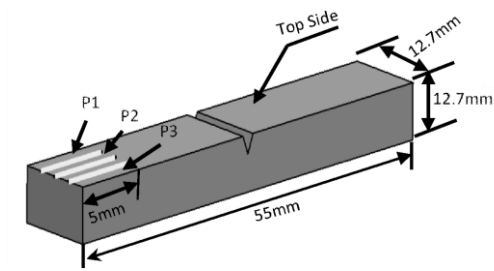

Figure 4: Specimen size and roughness test locations.

Each of the three CP PA-12 samples were coated with titanium prior to the electron microscope (SEM) scanning process. The SEM technique was used to examine the variations in coalescence and microstructure.

3D printing process

The operation setup consisted of three main stages: (i) pre-process stage (Figure 5 A-B), (ii) 3D printing process stage (Figure 5 C-D) and (iii) post-process stage (Figure 5 E-G). The SLS 3D printer has four main chambers: a feeder chamber, a building chamber, a collector chamber and a powder overflow chamber with roller for levelling (Figure 6). During the first stage, the material volume and weight were calculated using Materialise Magics software based on the quantity of the component that needed to be printed. In the 3D printing process stage, the primary constant parameters for the SLS 3D printer were set according to the configuration shown in Table 3. Next, during the post-processing stage, the material block was removed from the SLS

machine-building chamber and transferred to the sieve machine as shown in Figure 5 (E-G). Figure 5 (H) shows all the finished specimens that were ready for testing. Figure 6 shows the Farsoon model FS4092P SLS 3D printer which was used to produce all specimens with a maximum usable area of 350 x 350 x 400 mm.

Table 3: Experiment constant configuration SLS 3D printer

Properties	Value
Laser beam velocity	7.6 m/s
Layer thickness (LT)	0.06 mm
Hatch Distance	0.30 mm
Chamber temperature	169.5 °C
Laser power	70 Watt

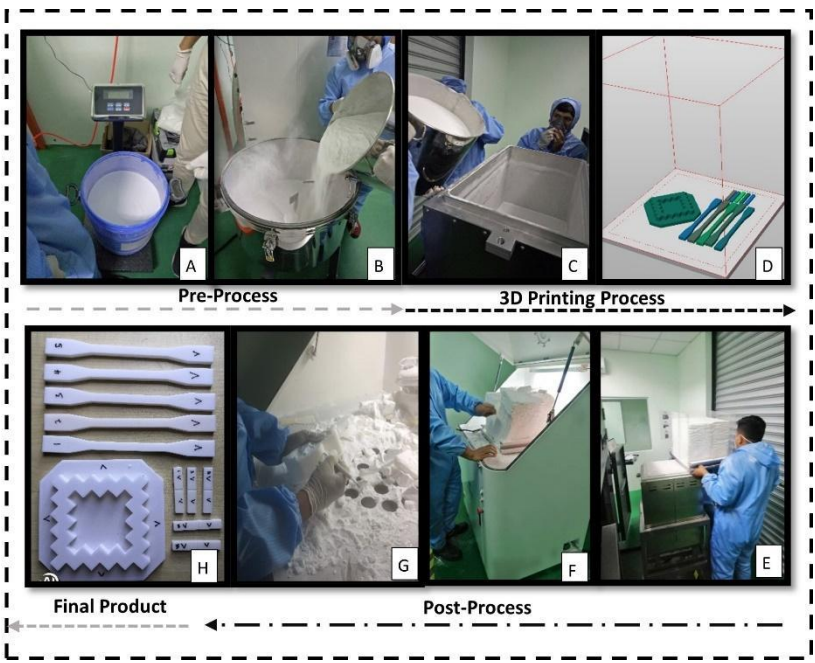

Figure 5: SLS 3D printing process flow.

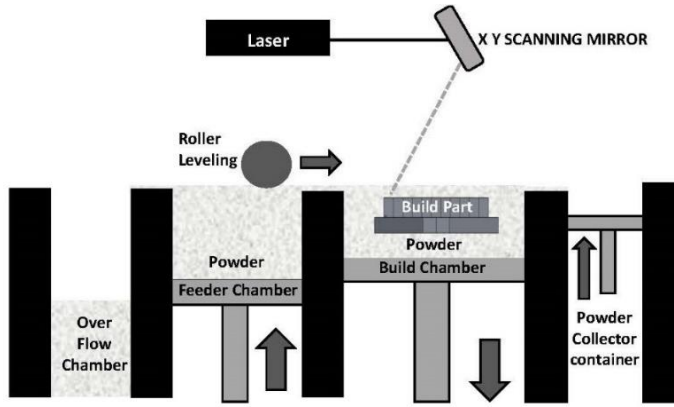

Figure 6: SLS process for Farsoon FS402P.

Test setup

The two main tests conducted for this study were the tensile strength and surface roughness. The INSTRON 600DX universal testing machine was used to test the tensile strength and material elongation. According to the ASTM D638 standard, the tensile was tested at a speed of v = 5 mm/min and a room temperature of 24 °C. These data were also useful in qualitative characterisation to identify a stiffer CP material.

Next, the measured surface roughness Ra, Rq and Rz values were obtained directly from the device's LCD display. The Mitutoyo SJ-410 machine was used as a table surface tester with a probe travelling length of 5 mm, a stylus tip radius of 2 mm and a detecting force of 4 mN. The measurement of point P1-P3 were repeated 3 times (N = 3) to ensure data precision.

A scanning electron microscopy (SEM) ZEISS EVO 18 was used to examine the morphology of the PA-12 different compositions; CP1, CP2 and CP3 sintered samples. The magnification setup was between 50 µm – 100 µm with an electron high tension (EHT) of 15 Kv, and the material microstructure were observed by scanning in the 2θ range of between 0 and 90°.

Results and Discussion

The most important key to obtaining a stiff material and a smooth surface is to understand the effects on the process parameters involved. Hence, the effects of the different material compositions on these process parameters were analysed in this section.

Material composition effect on tensile stress

Figure 7 shows the tensile stress versus strain graph for the three sample types with different material compositions; CP1, CP2 and CP3. CP1 showed a higher tensile strength with approximately 45.98 MPa and a strain rate of about 17.35%. Meanwhile, CP3 showed a lower tensile strength (approximately 36.28 MPa) than either CP 2 and CP 1. After being exposed to the laser beam more than two to three times, CP3 showed a reduced tensile strength indicating a change in the microstructure and the melting point of the material. According to Pilipović [7], CP1 should have a maximum tensile strength of between 40.74 and 46.44 MPa when subjected to varying chamber temperatures. However, this value is still lower than the manufacturer's maximum tensile test result. Yao [2] stated that recycled powder typically has a lower tensile strength due to adhesive bonding on the powder surfaces after the material was re-heated. This was consistent with the obtained results by CP2 and CP3. In addition, the laser power and scan spacing optimisation were also the influencing factors in obtaining tensile strength for CP1, CP2 and CP3 [19].

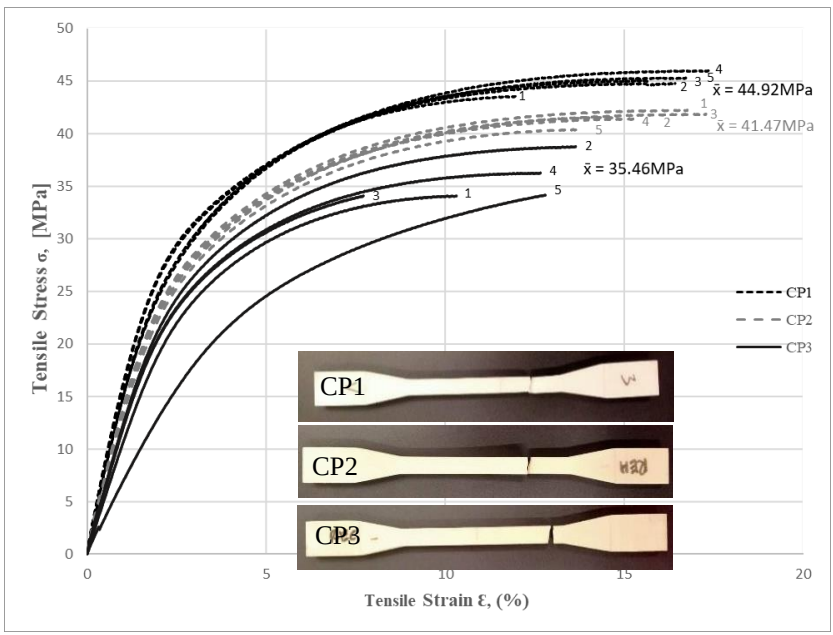

Figure 7: Tensile stress-strain with different material percentages.

Material composition effect on surface roughness

Figure 8 shows the significance of R_a values on the CP1, CP2 and CP3 samples. From three different measurement positions, the surface of CP1 was

found to be uniformly smooth with a total mean roughness of 10.75 µm. However. CP3 (100% recycle) was found to have a higher surface roughness than CP2 and CP1. Thus, the overall surface roughness conducted in this experiment produced better results of around 10-12 µm compared to the previous study conducted by Petzold [22]. Moreover, the surface roughness of the virgin and recycled material was in a range of 12-23 µm. Therefore, the study results inferred that the surface roughness was affected by the different CP material compositions. In addition, the part orientation also significantly affected the surface roughness of a prototype [23]. Referring to Figure 9, CP1 surface was smoother due to the bonding and spacing between the particles.

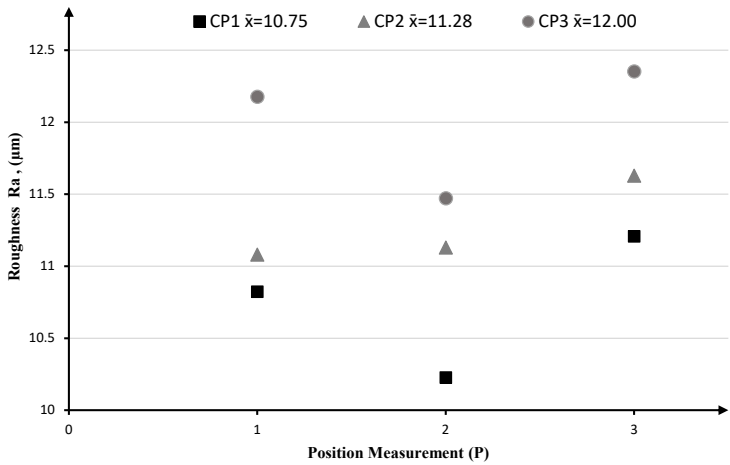

Figure 8: Surface roughness measurement.

PA-12 material composition morphology

The surface morphology of PA-12 powders with varying compositions is shown in Figure 9. The findings confirmed that the powder shape, size, and distribution were clearly different between the CP1, CP2, and CP3 materials. The CP1 result indicated that the powder shape and size were bonded to each other at the chamber temperatures ranging from 180 ºC to 190 ºC, sufficient to melt virgin powder [19]. Therefore, according to Dadbakhsh's study [19], the chamber temperatures for CP2 and CP3 must be increased in accordance with the melting points of mixed powder (180–200 °C) and aged powder (180–210 °C). The surface morphology of CP2 exhibited a high degree of porosity compared with CP1 and CP2. There were a few other distinct differences between the virgin powder and the adhered powder. The adhered powder melted when heated to a higher temperature, increasing the molecular chains

mobility. The powder shape changes to a sphere as a result of surface tension [20], whereas more fractured powder appeared in the adhered powder.

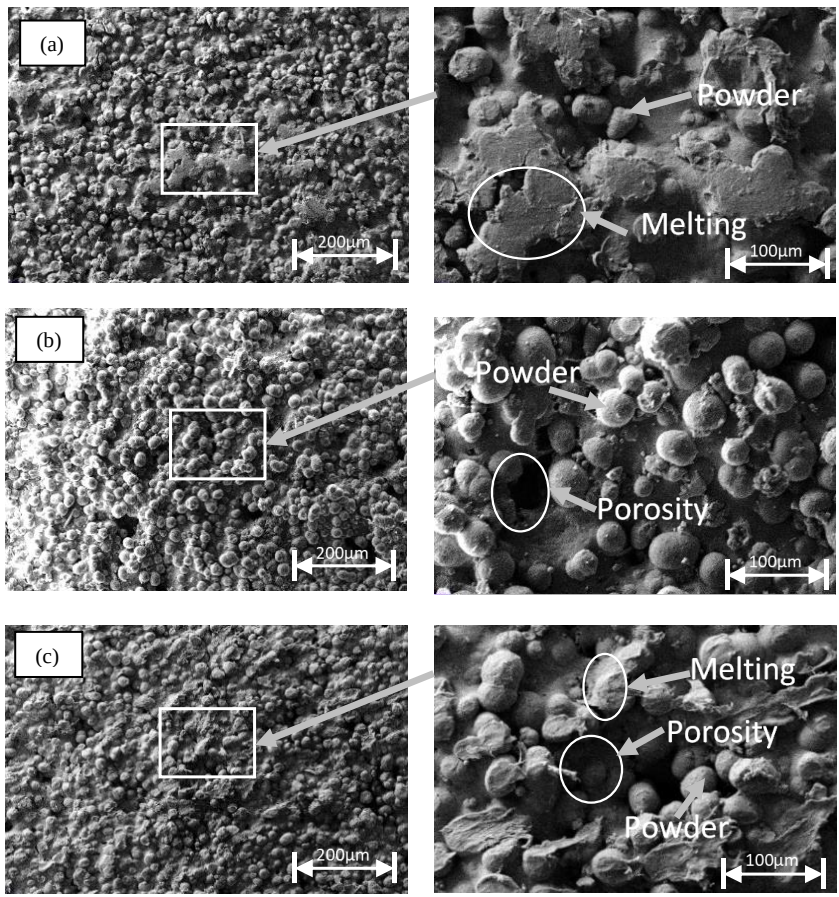

Figure 9: PA12 SEM images for (a) CP1, (b) CP2 and (c) CP3.

Conclusion

This research is advantageous as a guide for SLS 3D printer users who would like to print composite material products. The results of the study showed that the different PA-12 compositions had an effect on the mechanical properties and product surface quality during the SLS printing process. A CP1 with 100 percentage virgin material had higher tensile strength and a smoother surface

due to the high adhered powder content and the right melting point. The CP1 also consolidated rapidly during heating, in contrast to the CP2 and CP3, which morphed similarly to the CP1 but remained in the fully molten phase until at a significantly higher temperature (at which fully molten phase appeared). In general, the CP2 powder behaved similarly to the CP1 and CP3 powders. For future work, the recycled material will require a higher melting point depending on the previous recycling times and the increase in the amount of adhered powder.

Acknowledgement

The authors would like to thank Universiti Teknikal Malaysia Melaka, (UTeM) and Ministry of Education Malaysia for research grant [Grant Number FRGS/2018/FTKMP-CARE/F00385]

References

[1] R. Sinha, M. C. Torres, P. Scopece, E. V. Falzacappa, A. Patelli, L. Moroni, and C. Mota, "A hybrid additive manufacturing platform to create bulk and surface composition gradients on scaffolds for tissue regeneration," *Nature Communications*, vol. 12, no. 1, pp. 1-15, 2021.

[2] B. Yao, Z. Li, and F. Zhu, "Effect of powder recycling on anisotropic tensile properties of selective laser sintered PA2200 polyamide," *European Polymer Journal*, vol. 141, no. July, pp. 110093, 2020.

[3] T. D. Ngo, A. Kashani, G. Imbalzano, K. T. Q. Nguyen, and D. Hui, "Additive manufacturing (3D printing): A review of materials, methods, applications and challenges," *Composites Part B: Engineering*, vol. 143, pp. 172–196, 2018.

[4] W. Schneller, M. Leitner a, S. Leuders b, J.M. Sprauel, F. Grün, T. Pfeifer, and O. Jantschner, "Fatigue strength estimation methodology of additively manufactured metallic bulk material," *Additive Manufacturing*, vol 39, pp. 101688, 2021.

[5] W. D. Zhou and J. S. Chen, "3D printing of carbon fiber reinforced plastics and their applications," *Material Science Forum*, vol. 913, pp. 558–563, 2018.

[6] M. I. H. C. Abdullah, M. F. Abdollah, H. Amiruddin, N. Tamaldin, N. R. M. Nuri, and A. R. Saleman, "The hBN nanoparticles as an effective engine oil additive to enhance the durability and performance of a small diesel engine," *Journal of Mechanical Engineering*, vol. 1, pp. 103–112, 2017.

[7] A. Pilipović, T. Brajlih, and I. Drstvenšek, "Influence of processing parameters on tensile properties of SLS polymer product," *Polymers (Basel)*, vol. 10, no. 11, pp. 1-18, 2018.

[8] A. A. E. M. Nawi, M. I. H. C. Abdullah, and M. F. bin Abdollah, "Dispersion stability of hBN nanoparticle in liquid phase with different dispersion agents," *Journal of Mechanical Engineering*, vol. 15, no. 2, pp. 143–153, 2018.

[9] M. S. F. Hussin, M. R. Omar, K. A. Azlan, A. H. Azahar, Z. Ismail, and F. F. Rosli, "Orthopedic calf cast using antioxidative FS3200PA nylon 3D printing: Design and optimization," *ARPN Journal of Engineering and Applied Sciences*, vol. 14, no. 23, pp. 4093–4096, 2019.

[10] S. Mei, X. Zhang, Bowen Ding, J. Wang, P Yang, H. She, Z. Cui, M. Liu, X. Pang, and P. Fu, "3D-Printed thermoplastic polyurethane/graphene composite with porous segregated structure: Toward ultralow percolation threshold and great strain sensitivity," *Journal of Applied Polymer Science*, vol. 138, no. 14, pp. 1–11, 2021.

[11] S. Yuan, F. Shen, C. K. Chua, and K. Zhou, "Polymeric composites for powder-based additive manufacturing: Materials and applications," *Progress in Polymer Science*, vol. 91, pp. 141–168, 2019.

[12] A. Patel, V. Venoor, F. Yang, X. Chen, and M. J. Sobkowicz, "Evaluating poly (ether ether ketone) powder recyclability for selective laser sintering applications," *Polymer Degradation and Stability*, vol. 185, pp. 109502, 2021.

[13] Y. Yang, Y. Xu, S. Wei, and W. Shan, "Oral preparations with tunable dissolution behavior based on selective laser sintering technique," *International Journal of Pharmaceutics*, vol. 593, pp. 120127, 2021.

[14] K. Prasad, M. Obana, Y. Ishii, A. Ito, and S. Torizuka, "The effect of laser scanning strategies on the microstructure, texture and crystallography of grains exhibiting hot cracks in additively manufactured Hastelloy X," *Mechanics of Materials*, vol. 157, pp. 103816, 2021.

[15] I. Sagradov, D. Schob, R. Roszak, P. Maasch, H. Sparr, and M. Ziegenhorn, "Experimental investigation and numerical modelling of 3D printed polyamide 12 with viscoplasticity and a crack model at different strain rates," *Material Today Communication*, vol. 25, no. April, pp. 101542, 2020.

[16] Z. U, Y. Wang, D. Wu, K. P. Ananth, and J. Bai, "The process and performance comparison of polyamide 12 manufactured by multi jet fusion and selective laser sintering," *J. Manuf. Process.*, vol. 47, no. July, pp. 419–426, 2019.

[17] Farsoon Technologies, "Selective Laser Sintering Systems FARSOON 402P SERIES Break free with Farsoon Technologies," Man. B. farsoon sls 402P, 2017.

[18] F. Technologies, “General Properties FS 3401GB FS 3300PA,” pp. 2000–2001, 2001.
[19] N. Xu and C. C. Tutum, “Efficient sampling for design optimization of an SLS product,” *Solid Free. Fabr. 2017 Proc. 28th Annual International Solid Freeform Fabrication Symposium - An Addit. Manuf. Conf. SFF 2017*, pp. 951–962, 2020.
[20] J. W. Gooch, “Isobutylene,” in Encyclopedic Dictionary of Polymers, J. W. (Ed. Gooch, Ed. New York), NY: Springer New York, pp. 399, 2011.
[21] B. Yao, Z. Li, and F. Zhu, “Effect of powder recycling on anisotropic tensile properties of selective laser sintered PA2200 polyamide,” *European Polymer Journal*, vol. 141, pp. 110093, 2020.
[22] S. Petzold, J. Klett, A. Schauer, and T. A. Osswald, “Surface roughness of polyamide 12 parts manufactured using selective laser sintering,” *Polymer Testing*, vol. 80, pp. 1-12, 2019.
[23] H. Boejang, L. K. Lai, S. I. A. Kudus, M. R. Omar, M. I. F. Rosley, S. Mat, and M. R. Alkahari, “The influence of STL data quality on the surface roughness of 3D printed Melaka historical artifact,” *Proceedings of Mechanical Engineering Research Day*, pp. 47–48, 2020.